Journal of Alloys and Compounds 513 (2012) 499–505

Contents lists available at SciVerse ScienceDirect

Journal of Alloys and Compounds

journal homepage: www.elsevier.com/locate/jallcom

Preparation, characterization and catalytic effects of copper oxalate nanocrystals☆

Gurdip Singh*, Inder Pal Singh Kapoor, Reena Dubey, Pratibha Srivastava

Department of Chemistry, DDU Gorakhpur University, Gorakhpur 273009, India

ARTICLE INFO

Article history:
Received 1 June 2011
Received in revised form 22 October 2011
Accepted 29 October 2011
Available online 7 November 2011

Keywords:
Copper oxalate nanocrystals
Ammonium perchlorate
Composite solid propellants
Burning rate
Kinetics

ABSTRACT

Recent work has described the preparation and characterization of copper oxalate nanocrystals (CONs). It was characterized by X-ray diffraction (XRD), scanning electron microscopy (SEM), transmission electron microscopy (TEM), high resolution transmission electron microscopy (HRTEM) and electron diffraction pattern (ED). The catalytic activity of CONs on the thermal decomposition of ammonium perchlorate (AP) and composite solid propellants (CSPs) has been done by thermogravimetry (TG), differential scanning calorimetry (DSC) and ignition delay measurements. Burning rate of CSPs was also found to be enhanced in presence of copper oxalate nanocrystals. Kinetics of thermal decomposition of AP with and without CONs has also been investigated. The model free (isoconversional) and model-fitting kinetic approaches have been applied to data for isothermal TG decomposition.

1. Introduction

Composite solid propellants (CSPs) are the major source of chemical energy in space vehicles and missiles [1]. Ammonium perchlorate (AP) is one of the most common energetic material and oxidizer in CSPs. The thermal decomposition of AP plays a significant role in the burning behavior of propellants [2–4]. The characteristics of the thermal decomposition of AP are believed to influence the performance of CSPs and remarkably sensitive to additives [5–8]. The ballistics of CSPs can be improved by adding a catalyst such as Fe_2O_3, CuO, Cr_2O_3, and NiO; which accelerates the rate of decomposition of AP [9–11]. Recent investigations have shown that nanoparticles of transition metal [12] and ferrites [13,14] can catalyze the burning rate of CSPs. The thermal decomposition and combustion of CSPs are very complex, it is reasonable to wonder if adding another drop to the voluminous bucket of literature could possibly make any difference.

Nanocrystalline metal oxides, which represent the most diverse class of materials because of their unique structural, physical and chemical characteristics, are suitable for a variety of applications such as catalysts/photocatalysts, hydrogen storage materials, semiconductors, sensors, MRI contrast agents, and biomaterials. They have attracted tremendous attention because of their definite promise to revolutionize technologies of the future [15–18]. Metal oxalates are interesting candidates for nanostructured synthesis because these can be transformed to oxide or metals without losing the ordered structure [19]. A lot of works on the structure, properties and thermal behavior of metal oxalates are present in the literature [20]. Available evidence suggest that the oxalates of divalent transition metals are polymeric, with oxalate ion ($C_2O_4^{--}$) acting as a quadridentate bridging ligand and most such oxalates are isomorphous. The thermal decomposition of copper oxalate differs substantially from that of the other transition metal oxalates [21].

The goal of the study is to prepare, characterize copper oxalate nanocrystals (CONs) and investigate its catalytic effect on the thermal decomposition of AP, CSPs and burning rate of CSPs.

2. Experimental procedure

2.1. Materials

AP obtained from CECRI, Karaikudi; $Cu(NO_3)_2{\cdot}2H_2O$ (Merck), oxalic acid (Merck), HTPB (VSSC, Thiruvanthapuram), IPDI (Merck) and DOA (Merck) were used as received without further purification.

2.2. Preparation of copper oxalate nanocrystals (CONs)

In a typical procedure, 0.04 mol/L solutions of $Cu(NO_3)_2{\cdot}2H_2O$ (0.892 g) and oxalic acid (0.36 g) in 100 mL acetone were mixed together to obtain a colloidal suspension of CONs. The suspension was kept under permanent stirring and the temperature was regulated to 40 °C. The suspension was vacuum filtered, dried at 80 °C for 12 h then washed with ethanol, finally filtered and dried again at 80 °C for 12 h [22] to get CuC_2O_4 nanocrystals.

☆ Part 78.

* Corresponding author. Tel.: +91 551 2200745 (R/H)/2202856 (O); fax: +91 551 2340459.
E-mail address: gsingh4us@yahoo.com (G. Singh).

0925-8388/$ – see front matter © 2011 Elsevier B.V. All rights reserved.
doi:10.1016/j.jallcom.2011.10.100

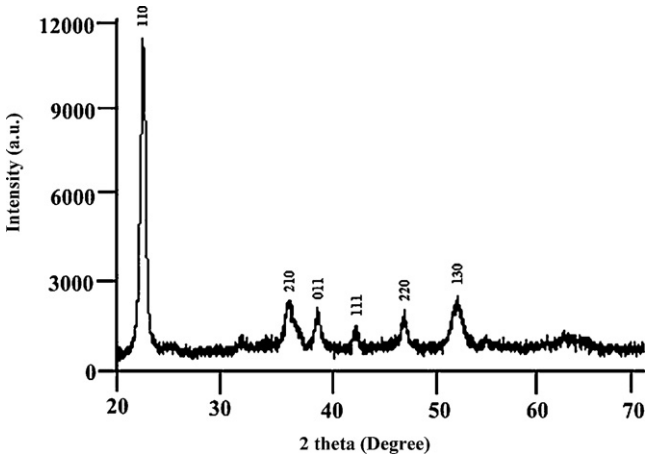

Fig. 1. XRD pattern of CuC_2O_4 nanocrystals.

2.3. Characterizations

XRD (Fig. 1) measurements were performed on a Bruker AXSD8 advance X-ray diffractometer using Cu K_α ($\lambda = 1.5418$ Å) radiation. The size and morphology of the sample was observed by field emission scanning electron microscope (FE-SEM) (Fig. 2a) and JEOL JEM transmission electron microscope (TEM) (Fig. 2b), high resolution transmission electron microscope (HR-TEM) (Fig. 2c) and selected area diffraction (SAED) pattern (Fig. 2d and e).

2.4. Preparation of CSPs

CSPs samples were prepared by dry mixing [23] of AP [100–200 mesh] with CONs (1% by wt) followed by addition of hydroxyl terminated polybutadiene (HTPB). The ratio of AP:HTPB was taken as 3:1. The binder part includes the curing agent isophoron diisocynate (IPDI), in equivalent ratio to HTPB, and plasticizer dioctyl adipate (DOA), 30% to HTPB. During mixing of the solid components with HTPB, temperature was maintained at 60 °C for 1 h. The propellants were prepared with and without nanocrystals, casted into aluminum plates having dimensions 1 cm × 3 cm × 10 cm. The samples were cured in an incubator at 70 °C for 8–10 days [11].

3. Catalytic activity

3.1. Burning rate measurements

The burning rate of CSPs was measured in the manner reported earlier [11,24,25]. The propellant strands were inhibited by applying PVC tape to check the side burning. The strands were held vertically and ignited electrically with the help of a nichrome wire at the top. The time required for a certain length of burning of the strand was recorded by a stop watch. The burning rate has been calculated by taking l/t, where l is length of propellant strand (cm) and t the time (s) of burning. An average of 3 measurements was taken within experimental error and results are reported in Table 1.

3.2. Thermal decomposition

Thermal decomposition was investigated as follows.

Table 1
Burning rate of CSPs with and without CuC_2O_4 nanocrystals (1 wt%).

Additive	Burning rate (mm/s)	$r_{bc}/r_b{}^*$
Nil	1.15	1.00
CuC_2O_4	1.65	1.43

r_b and $r_b{}^*{}_c$ = burning rate of propellant with and without CuC_2O_4 nanocrystals, respectively.

3.2.1. Simultaneous TG-DSC

TG-DSC thermogram (Fig. 3) on pure AP and AP with CONs (by mixing in ratio of 99:1) were recorded on the samples (~12 mg) using Perkin Elmer (Pyris Diamond) in the temperature range of room temperature to 600 °C under nitrogen atmosphere (flow rate 200 mL/min) at a heating rate of 10 °C min^{-1} in an open alumina pan.

3.2.2. Non-isothermal TG in static air

Non-isothermal TG studies on AP and HTPB-AP (CSPs) with and without nanocrystals (wt ~ 20 mg) were undertaken in static air at the heating rate of 10 °C min^{-1} using an indigenously fabricated TG apparatus [26]. A round bottom gold crucible was used as the sample holder. The percentage mass loss has been plotted against temperature (°C) and the curves are shown in Fig. 4.

3.2.3. Isothermal TG

The isothermal TG of AP with and without CONs (wt ~ 20 mg) was taken in static air using the above said TG apparatus at appropriate temperatures (Fig. 5).

3.2.4. Kinetic analysis of isothermal TG data

Kinetic analysis of thermal decomposition of AP is usually based on a single-step kinetic equation (1) [27]

$$\frac{d\alpha}{dt} = k(T)f(\alpha) \tag{1}$$

where t is the time, T is the temperature, α is the extent of conversion ($0 < \alpha < 1$), $k(T)$ is the rate constant, and $f(\alpha)$ is the reaction model [27], which describes the dependence of the reaction rate on the extent of reactions. The value of α is experimentally derived from the global mass loss in TG experiments. The reaction model may take various forms. The temperature dependence of $k(T)$ can be satisfactorily described by the Arrhenius equation, when substitution into Eq. (1) yields

$$\frac{d\alpha}{dt} = A \exp\left(-\frac{E}{RT}\right) \cdot f(a) \tag{2}$$

where A is pre exponential factor, E activation energy and R the gas constant.

3.2.4.1. Model fitting method. Rearrangement and integration of Eq. (1) for isothermal conditions gives

$$g_j(a) = k_j(T)t \tag{3}$$

where $g(\alpha) = \int_0^\alpha [f(\alpha)]^{-1} d\alpha$ is the integrated form of the reaction model. The subscript j has been introduced to emphasize that substituting a particular reaction model in Eq. (3) results in evaluating the corresponding rate constant, which is determined from the slope of a plot of $g_j(\alpha)$ verses t. For each reaction model selected, the rate constants are evaluated at several temperatures T_i and Arrhenius parameters are determined using the Arrhenius equation (4) in its logarithmic form

$$\ln\ k_j(T_i) = \ln A_j - \frac{E_j}{RT_i} \tag{4}$$

Arrhenius parameters were evaluated for isothermal experimental data by the model fitting method.

3.2.4.2. Isoconversional method. This method allows the activation energy to be evaluated without making any assumptions about the reaction model. Additionally, the method evaluates the effective

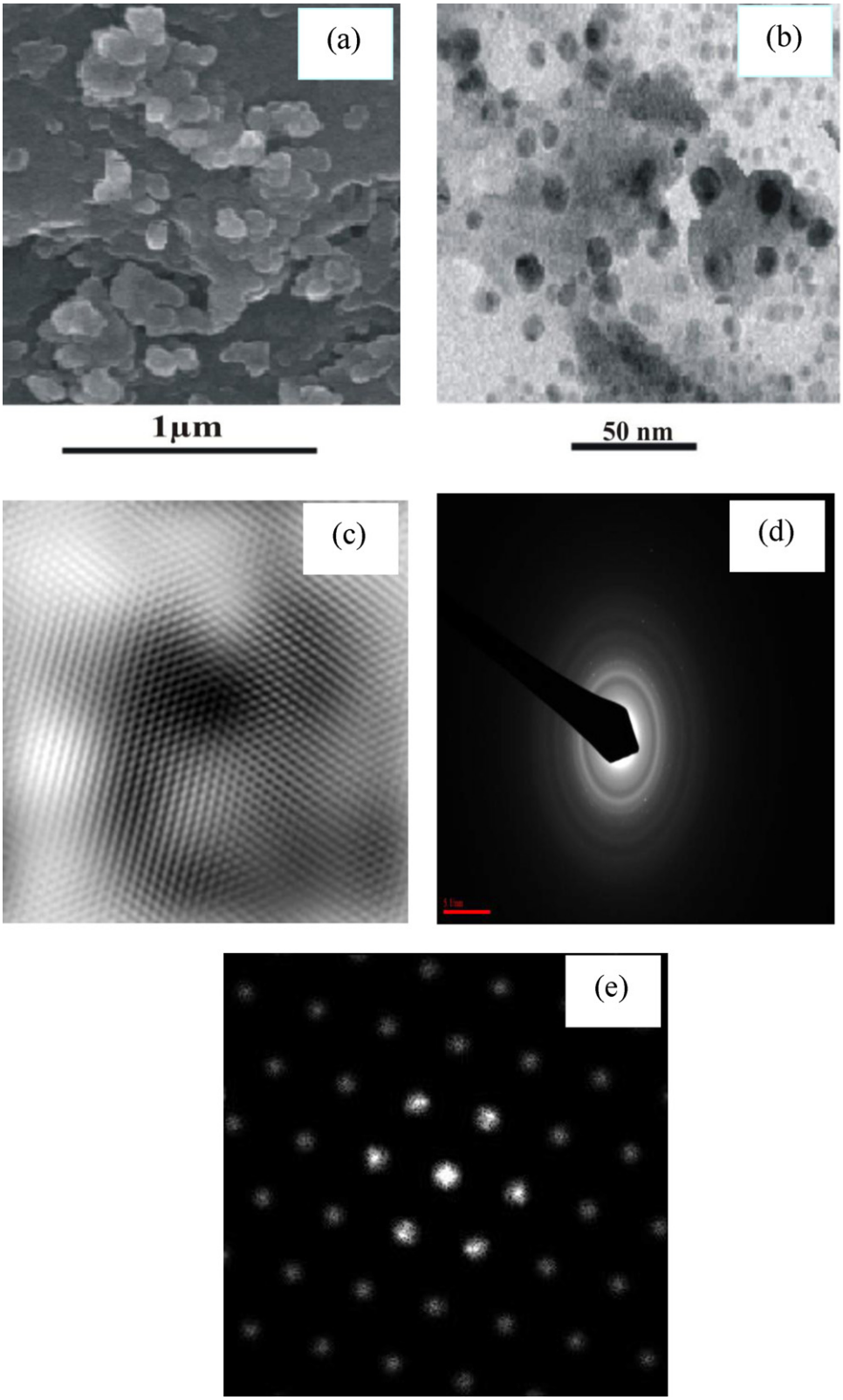

Fig. 2. Microstructural image of CONs (a) FE-SEM images, (b) bright field TEM micrographs, (c) HRTEM images, and (d, e) SEAD pattern of CuC_2O_4 nanocrystals.

activation energy as a function of the extent of conversion which allows one to explore multistep kinetics.

The basic assumption of the isoconversional method [28] is that the reaction model as defined in Eq. (1) is not dependent on temperature or heating rate. Under isothermal conditions, on combining Eqs. (3) and (4) we get,

$$-\ln\ t_{\alpha,i} = \ln\frac{A_\alpha}{g(\alpha)} - \frac{E_\alpha}{RT_i} \tag{5}$$

where E_α is evaluated from the slope of the plot of $-\ln t_{\alpha,i}$ against T_i^{-1}. Thus, E_α at various α_i for AP with and without CNOs have been evaluated and the E_α dependencies are shown in Fig. 6.

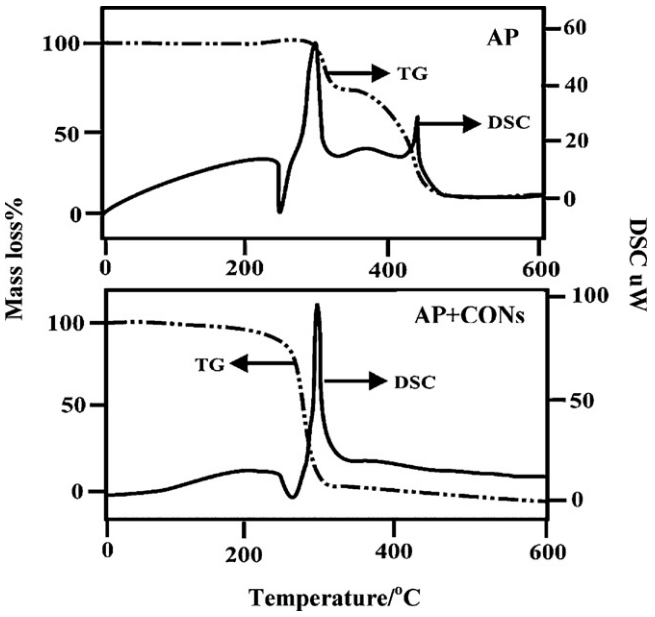

Fig. 3. TG-DSC curves of AP with and without 1% CuC_2O_4 nanocrystals in nitrogen atm.

3.3. Ignition delay measurements

The ignition delay (D_i) measurements were made on 20 mg samples (100–200 mesh) by using a tube furnace technique [29] in the temperature range 360–420 °C. The accuracy of the temperature of tube furnace was ±1 °C. The sample was taken in an ignition tube (5 cm length × 0.4 cm diameter) and the time interval between the insertion of the ignition tube into the TF and the moment of appearance of a flame noted with the help of a stop watch with accuracy of 0.1 s gave the value of ignition delay (D_i). The ignition tube clamped in a bent wire was inserted manually into the furnace up to a fix depth (14 cm) just above the probe of the temperature indicator cum controller (Century, Chandigarh). The time for insertion of the ignition tube was also kept constant. Each run was repeated three times, and mean D_i values are reported in Table 2. The D_i data were found to be fit in equation [30–32],

$$D_i = A \exp\left(\frac{E_a^*}{RT}\right) \quad (6)$$

where D_i is a time of ignition (ignition delay), A is constant, E_a^* is the energy of activation (ignition) and T is the absolute temperature.

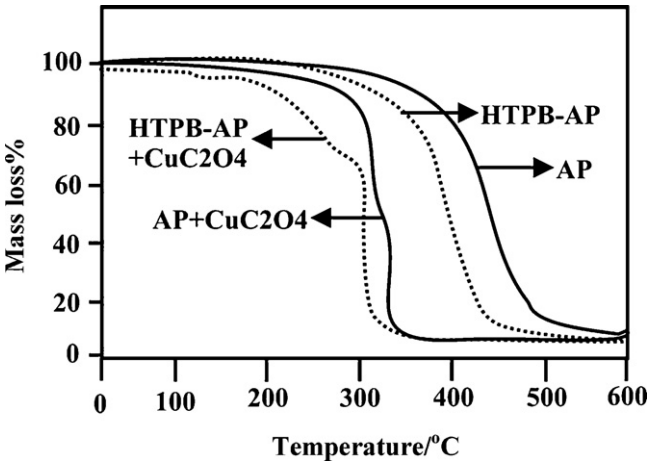

Fig. 4. TG curves of AP and CSPs with and without CuC_2O_4 nanocrystals.

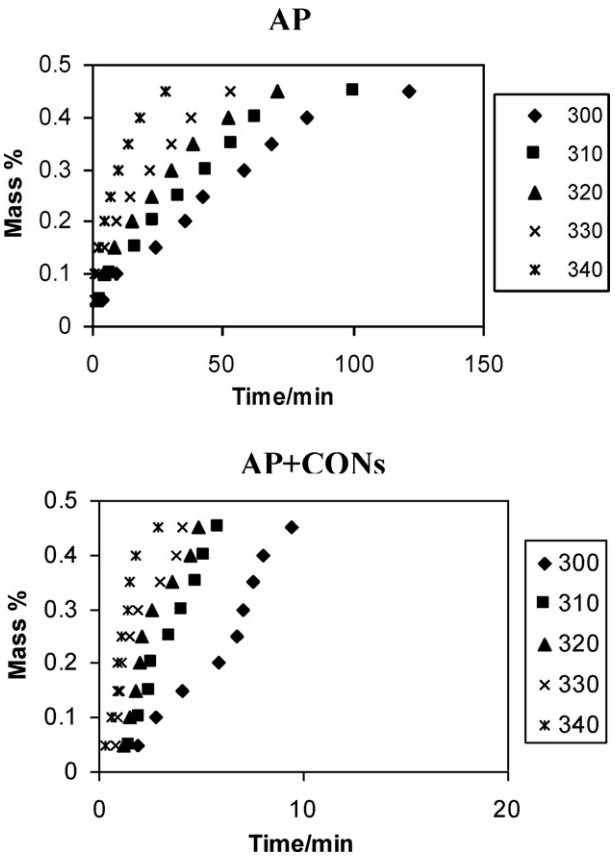

Fig. 5. Isothermal TG of AP and AP + CuC_2O_4 (1% by wt) on different temperatures.

This equation has been found to be obeyed by a large number of explosives [33–38]. E_a^* assessed by above equation along with the correlation coefficient (r) are given in Table 2.

4. Results and discussion

4.1. XRD analysis

Fig. 1 shows the structural characteristics of CONs investigated by XRD. These studies reveal that the CONs obtained by colloidal suspension of $Cu(NO_3)\cdot 2H_2O$ and oxalic acid in acetone are crys-

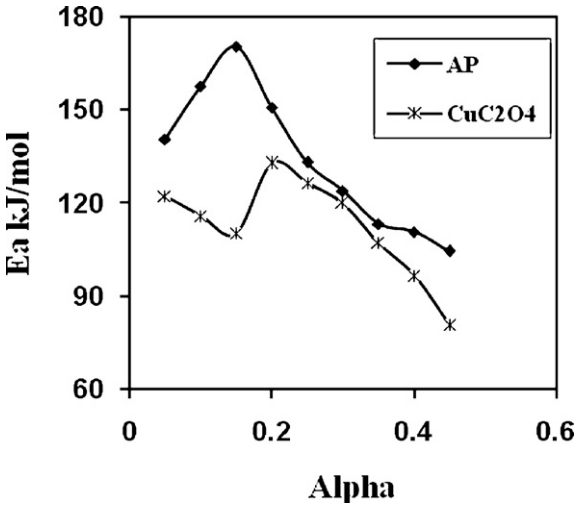

Fig. 6. Dependencies of activation energy on the extent of conversion α.

Table 2
Ignition delay (D_i), activation energy for ignition (E_a) and correlation coefficient of AP and CSPs with and without CuC_2O_4 nanocrystals.

Sample	D_i (s)					E_a (kJ mol^{-1})	r (correlation coefficient)
	360 ± 1 °C	375 ± 1 °C	390 ± 1 °C	405 ± 1 °C	420 ± 1 °C		
AP	105	93	85	71	60	33.7	0.9885
AP + CuC_2O_4(1 wt%)	65	60	52	46	43	26.6	0.9939
HTPB-AP	95	82	72	68	59	27.7	0.9930
HTPB-AP + CuC_2O_4 (1 wt%)	60	58	54	45	43	22.3	0.9637

talline. The broadening of the peaks indicates nanometer size of the products and no peak of impurity was observed in XRD pattern. The relative crystalline sizes are determined from the XRD line broadening using the Scherrer equation,

$$d = \frac{0.9\lambda}{\beta \cos \theta}$$

where d is the crystallite size, λ is the wavelength used in XRD (1.5418 Å), θ the Bragg angle, β is the pure diffraction broadening of a peak at half height, i.e., broadening due to crystallite dimensions.

The size of CONs is estimated to be 12.4 nm according to the Scherrer equation [39–41]. The XRD analysis when compared with the standard data for CONs (JCPDS No. 21-0297) reveals the presence of a cubic phase (a = 5.40, b = 5.57, c = 2.54). The most intense peak (intensity 100) is from the plane which corresponds to an angle of 2θ = 22.9.

4.2. Microstructural studies

For microstructural studies the FE-SEM and TEM images of as prepared CONs are presented in Fig. 2a and b. The FE-SEM image (Fig. 2a) of CONs reveals that the crystals are spherical in shape with narrow size distribution. Moreover, the particle size was found to lay in the range 9–25 nm. The size of the particles observed in the TEM image (Fig. 2b) is in the range of 9–12 nm, which is in good agreement with that estimated by Scherrer equation. The TEM images reveal that there is no agglomeration in the crystals of the CONs. The HRTEM images reveal that the CONs are single crystals. As shown in Fig. 2d and e, the selected area electron diffraction pattern has many widen diffraction rings made up of many diffraction spots which also indicate the nanocrystallinity of the CONs.

4.3. Thermal analysis

The results of TG-DSC (Fig. 3) and TG (Fig. 4) on AP with and without CONs (1% by wt) shows that rate of decomposition of AP is increased by CONs. The DSC curve for AP (Fig. 3) shows three events. The first endothermic DSC peak at 244 °C represents the transition from orthorhombic to cubic AP [42,43]. The second exothermic peak at 307 °C is accompanied by a weight loss of 29% and corresponds to the partial decomposition of AP and formation of an intermediate. The third main exothermic peak at about 414 °C is associated with 70.5% weight loss. This corresponds to the complete decomposition of the intermediate to volatile products. The DSC curves of AP in presence of CONs show noticeable changes in the decomposition pattern. From Fig. 3, it is clear that CONs have no effect on crystallographic transition temperature (244 °C) of AP (the endotherm), while large decrease of 130 °C was observed in high temperature exothermic peak where two exothermic peaks of AP were merge to give only one.

The non-isothermal TG on AP (Fig. 4) shows two steps [44,45]. AP on heating first loses 25% of its mass at around 300 °C, i.e., low temperature decomposition (LTD). Beyond this temperature a plateau is observed; AP loses 80% of its mass at around 450 °C, i.e., high temperature decomposition (HTD). Experimental observation indicates that CONs affect both LTD and HTD of AP.

Fig. 4 clearly indicates that the thermal decomposition of AP and CSPs is catalyzed by CONs. Burning rate of CSPs has also been enhanced by this catalyst (Table 1). It is reported [21] that CuC_2O_4 incorporates little or no water of crystallization in its crystal lattice, which makes its decomposition not preceded by the disruption of the crystal lattice caused by dehydration. The thermal decomposition of CONs in O_2 atmosphere corresponds to strongly exothermic reaction, owing to the reaction of evolved CO with oxygen to form CO_2 and the oxidation of the Cu decomposition product to a copper oxide. Copper oxalate is anhydrous and the TG curve showed only one decomposition step with onset at about 305 °C due to breaking of a C–O bond and a C–C bond of $C_2O_4^{--}$ on, to form CuO (a black solid slightly soluble in acidic (pH ≈ 6.0) water) as;

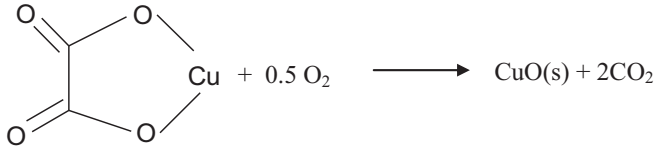

Cu metal was not found to be formed on thermal decomposition of CONs. The X-ray diffraction peaks of residue left after the thermal decomposition of CONs with AP is quite identical to those of pure CuO (Fig. 7), which can be indexed as the monoclinic structure CuO (a = 4.68 Å, b = 3.42 Å, c = 5.12 Å). The diffraction data are in agreement with JCPDS card of CuO (JCPDS file No. 41-0254). According to the Scherrer equation, the size of nano CuO was found to be 15 nm.

Copper oxide has a finer particle size with a large number of defects and dislocations in the crystal lattice. Thus, a large number of active sites would be available for the adsorption of reactants and consequently increases the rate of reaction. The catalytic activity of CONs in the thermolysis of AP and CSPs is measured by ignition delay [11]. Ignition delay data given in Table 2 show that the time required for ignition and activation energy for thermal ignition is lowered by adding CONs in AP and CSPs. The process of ignition [46] can never be treated as steady-state since it is a transient process prior to sustained combustion.

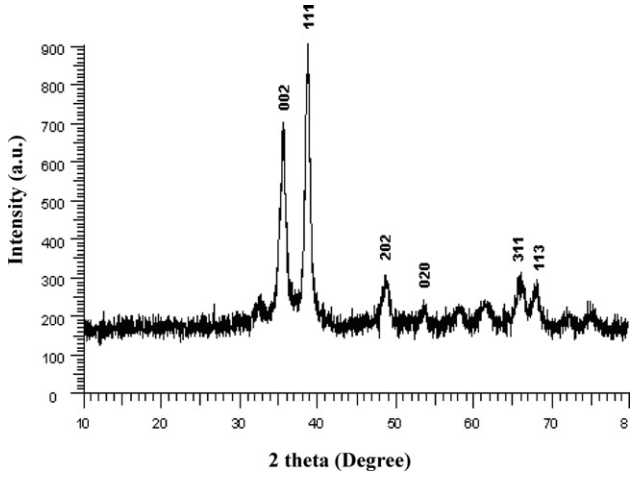

Fig. 7. XRD pattern of CuO nanocrystals.

Table 3
Set of reaction models applied to describe thermal decomposition of solids.

Model No.	Reaction model	$f(\alpha)$	$g(\alpha)$
1	Power law	$4\alpha^{3/4}$	$\alpha^{1/4}$
2	Power law	$3\alpha^{2/3}$	$\alpha^{1/3}$
3	Power law	$2\alpha^{1/2}$	$\alpha^{1/2}$
4	Power law	$2/3\alpha^{-1/2}$	$\alpha^{3/2}$
5	One-dimensional diffusion	$1/2\alpha^{-1}$	α^{2}
6	Mampel (first order)	$1-\alpha$	$-\ln(1-\alpha)$
7	Avrami-Erofeev	$4(1-\alpha)[-\ln(1-\alpha)]^{3/4}$	$[-\ln(1-\alpha)]^{1/4}$
8	Avrami-Erofeev	$3(1-\alpha)[-\ln(1-\alpha)]^{2/3}$	$[-\ln(1-\alpha)]^{1/3}$
9	Avrami-Erofeev	$2(1-\alpha)[-\ln(1-\alpha)]^{1/2}$	$[-\ln(1-\alpha)]^{1/2}$
10	Contracting sphere	$3(1-\alpha)^{2/3}$	$1-(1-\alpha)^{1/3}$
11	Three-dimensional diffusion	$2(1-\alpha)^{2/3}[1-(1-\alpha)^{1/3}]^{-1}$	$[1-(1-\alpha)^{1/3}]^{2}$
12	Contracting cylinder	$2(1-\alpha)^{1/2}$	$1-(1-\alpha)^{1/2}$
13	Prout-Tompkins	$\alpha/(1-\alpha)$	$\ln(\alpha/1-\alpha)$
14	Ginstling-Brounshtein	$3/2[(1-\alpha)^{-1/3}-1]^{-1}$	$[1-(2\alpha/3)]-(1-\alpha)^{2/3}$

Table 4
Activation energy (E_a), Arrhenius parameters and correlation coefficient (r) for the isothermal decomposition of AP and AP with copper oxalate nanocrystals.

Model No.	AP			AP + CuC_2O_4		
	E_a (kJ mol^{-1})	r	$-\ln A$	E_a (kJ mol^{-1})	r	$-\ln A$
1	94.69	0.9619	13.8	66.42	0.9166	10.8
2	95.00	0.9622	14.1	67.06	0.9192	11.1
3	95.60	0.9627	14.3	68.32	0.9239	11.5
4	98.48	0.9646	14.6	75.53	0.9407	12.6
5	99.46	0.9648	14.4	78.66	0.9446	12.9
6	97.97	0.9641	15.1	74.39	0.9383	13.1
7	97.06	0.9641	14.6	70.85	0.9344	12.0
8	95.64	0.9626	14.4	68.59	0.9240	11.6
9	96.29	0.9631	14.7	70.07	0.9286	12.1
10	97.72	0.9640	13.8	73.60	0.9371	11.7
11	100.22	0.9625	12.8	80.74	0.9442	11.5
12	97.59	0.9640	14.2	73.21	0.9364	11.9
13	102.06	0.9801	17.5	68.57	0.9389	13.4
14	88.57	0.9288	10.3	45.68	0.8548	4.4

Fourteen reaction models (Table 3) [27,47] were used to analyze isothermal TG data (in the range 300–340 °C, Fig. 5) to calculate the E_a values for thermal decomposition of AP and AP + CONs. The activation energy (E_a) values, Arrhenius parameters and correlation coefficients are reported in Table 4. The kinetics is analyzed by choosing a best fit model based on the value of correlation coefficient 'r' close to 1. Among the various values of r, calculated for different models; the highest value of r for AP corresponds to model 13, i.e., Prout-Tompkins and AP with CONs corresponds to model 5, i.e., the rate controlling process in the thermal decomposition respectively being chain growth of nuclei and one-dimensional diffusion. The corresponding values of E_a calculated for AP and AP + CONs are 102.1 and 78.7 kJ mol^{-1}, respectively (Table 4). The results of kinetic analysis confirm that incorporation of CONs, cause a noticeable decease in activation energy and consequently CONs act as catalyst.

The isoconversional method [28,48–51] is known to permit estimation of the apparent activation energy, independent of the model, corresponding to extent of conversion of the sample. This method allows the activation energy to be evaluated without making any assumptions about the reaction model. Additionally, the method evaluates the effective activation energy as a function of conversion which allows one to explore multistep kinetics. Though, model fitting method using a set of reaction model applied to isothermal data but model free approach (isoconversional method) is a better method of obtaining reliable and consistent kinetic information [52].

According to Fig. 6, each activation energy has a separate value at different α's for both AP and AP + CONs. Kinetic analysis performed by the isoconversional method on thermogravimetric data (Fig. 6) is consistent with the fact that thermal decomposition of AP and AP + CONs has an initial overall activation energy of 140.5 and 122.2 kJ mol^{-1}, respectively. These values decrease with the extent of conversion to about 104.5 and 80.8 kJ mol^{-1}, respectively, for AP and AP + CONs at the end of reactions.

A number of reactions have been reported [53,54] to be involved in the decomposition and combustion of AP because of the four elements and the full range of oxidation states utilized by nitrogen and chlorine. The breaking of an N–H bond, then proton transfer from NH_4^+ to ClO_4^- to form an O–H bond leads to the formation of NH_3 and $HClO_4$ in a primary step in condense phases [55].

$$\underset{(I)}{NH_4^+ + ClO_4^-} \rightarrow \underset{(II)}{NH_3\text{–}H\text{–}ClO_4} \rightarrow \underset{(III)}{NH_3\text{–}HClO_4} \rightarrow NH_3(a) + HClO_4(a) \rightarrow NH_3(g) + HClO_4(g)$$

Further secondary reactions occur at higher temperature through complex competitive steps to produce gaseous products.

5. Conclusion

The narrow size distribution of CONs is in agreement with the result of XRD, SEM and TEM. TG-DSC and kinetic studies reveals that the CONs have good catalytic effect on thermal decomposition of AP and CSPs. The model free (isoconversional) and model-fitting kinetic approaches have shown that rate of decomposition of AP increases with CONs. Ignition delay and burning rate of CSPs were also found to be enhanced with CONs.

Acknowledgements

The authors are grateful to Head, Chemistry Department of DDU Gorakhpur University for laboratory facility and IIT Roorkee for TG-DSC. Thanks are also due to financial assistance by UGC for providing Emeritus Fellow to G. Singh and Project Fellowship to Reena Dubey.

References

[1] P.W.M. Jacob, H.M. Whitehead, Chem. Rev. 69 (1969) 551.
[2] V.V. Boldyrev, Thermochim. Acta 443 (2006) 1.
[3] V.G. Dedgaonkar, D.B. Sarwade, J. Therm. Anal. 36 (1990) 223.
[4] P.R. Patil, V.N. Krishnamurthy, S.S. Joshi, Propell. Explos. Pyrot. 33 (2008) 266.
[5] G. Singh, I.P.S. Kapoor, S. Dubey, P.F. Siril, J. Sci. Conf. Proc. 1 (2008) 7.
[6] G. Singh, I.P.S. Kapoor, S. Dubey, P.F. Siril, Propell. Explos. Pyrot. 34 (1) (2009) 72.
[7] J. Zhu, D. Li, H. Chan, X. Yang, L. Lu, X. Wang, Mater. Lett. 58 (2004) 3324.
[8] L. Liu, F. Li, L. Tan, L. Miang, Y. Yi, Propell. Explos. Pyrot. 1 (2004) 29.
[9] A.A. Said, Therm. Anal. 37 (1991) 959.
[10] F. Solymosi, E. Krix, J. Catal. 1 (1962) 468.
[11] G. Singh, S.P. Felix, Combust. Flame 132 (2003) 422.
[12] G. Singh, I.P.S. Kapoor, S. Dubey, J. Alloys Compd. 480 (2009) 270.
[13] G. Singh, I.P.S. Kapoor, S. Dubey, S.P. Flix, J.H. Yi, F.Q. Zhao, R.J. Hu, Thermochim. Acta 477 (2008) 42.
[14] P. Srivastava, I.P.S. Kapoor, G. Singh, J. Alloys Compd. 485 (2009) 88.
[15] B. O'Regan, M. Gratzel, Nature 353 (1991) 737.
[16] A. Fujishima, T.N. Rao, D.A. Tryk, J. Photobiol. C: Photochem. Rev. 1 (2000) 1.
[17] T. Rajh, Z. Saponjic, J. Liu, N.M. Dimitrijevic, N.F. Scherer, M. Vega-Arroyo, P. Zapol, L.A. Curtiss, M.C. Thurnauer, Nano Lett. 4 (2004) 1017.
[18] H. Tokuhisa, P.T. Hammond, Adv. Funct. Mater. 13 (2003) 831.
[19] L. Cristina Soare, P. Bowen, J. Lemaitre, H. Hofmann, J. Phys. Chem. B 110 (2006) 17763.
[20] D. Dollimore, Thermochim. Acta 117 (1987) 331.
[21] A. Coetzee, D.J. Eve, M.E. Brown, J. Therm. Anal. 39 (1993) 947.
[22] J. Romann, V. Chevallier, A. Merien, J.C. Valmalette, J. Phys. Chem. C 113 (2009) 5068.
[23] S. Krishna, R.D. swami, J. Propul. Power 13 (2) (1997) 207.
[24] R.P. Rastogi, G. Singh, B.L. Dubey, C.S. Shukla, J. Catal. 65 (1980) 25.
[25] R.P. Rastogi, G. Singh, R.R. Singh, Combust. Flame 33 (1978) 305.
[26] G. Singh, R.R. Singh, Res. Ind. 23 (1978) 92.
[27] M.E. Brown, D. Dollimore, A.K. Galway, Comprehensive Chemical Kinetics, vol. 22, Elsevier, Amsterdam, The Netherlands, 1960.
[28] S.V. Vyazovkin, Int. J. Chem. Kinet. 28 (1996) 95.
[29] G. Singh, S.K. Vasudeva, I.P.S. Kapoor, Indian J. Technol. 29 (1991) 589.
[30] N. Semenov, Chemical Kinetics and Chain Reactions, vol. 18, Clarendon Press, Oxford, UK, 1935.
[31] E.S. Freeman, S. Gordon, J. Phys. Chem. 60 (1956) 867.
[32] J. Zinn, R.N. Rogers, J. Phys. Chem. 66 (1962) 2646.
[33] G. Singh, B.P. Baranwal, I.P.S. Kapoor, D. Kumar, C.P. Singh, R. Frohlich, J. Therm. Anal. Calorim. 91 (3) (2008) 971.
[34] G. Singh, B.P. Baranwal, I.P.S. Kapoor, D. Kumar, R. Frohlich, J. Phys. Chem. A 111 (2007) 12972.
[35] G. Singh, R.R. Singh, A.P. Rai, I.P.S. Kapoor, J. Therm. Anal. 36 (1990) 2539.
[36] G. Singh, I.P.S. Kapoor, D. Kumar, U.P. Singh, N. Goel, Inorg. Chim. Acta 362 (2008) 4091.
[37] H. Henkin, R. McGill, Ind. Eng. Chem. 44 (1952) 1391.
[38] K. Singh, Trans. Faraday Soc. 55 (1959) 124.
[39] X. Lu, X. Wang, J. Zhang, L. Lu, Thermochim. Acta 342 (1999) 97.
[40] L.S. Birks, H. Friedman, J. Appl. Phys. 17 (1946) 687.
[41] E. Lamprecht, G.M. Watkins, M.E. Brown, Thermochim. Acta 446 (2006) 91.
[42] K. Kishore, K. Sridhara, Solid Propellant Chemistry: Condense Phase Behavior of Ammonium Perchlorate Based Solid Propellants, DESIDOC, New Delhi, 1999, p. 10.
[43] F. Solymosi, Acta Phys. Chem. 20 (1974) 1.
[44] L.L. Bircumshaw, B.H. Newmann, Proc. Roy. Soc., A 227 (1954) 115.
[45] P.W.M. Jacobs, G.S. Pearson, Combust. Flame 13 (1969) 419.
[46] B.L. Hicks, J. Chem. Phys. 66 (1962) 2646.
[47] S. Vyazovkin, I. Dranca, X. Fan, R. Advincula, Macromol. Rapid Commun. 25 (2004) 498.
[48] I.P.S. Kapoor, P. Srivastava, G. Singh, U.P. Singh, R. Frohlich, J. Phys. Chem. A 112 (2008) 652.
[49] S. Vyazovkin, C.A. Wight, Chem. Mater. 11 (1999) 3386.
[50] A.J. Lang, S. Vyazovkin, Combust. Flame 145 (2006) 779.
[51] S. Vyazovkin, C.A. Wight, Thermochim. Acta 340 (1999) 53.
[52] S. Vyazovkin, A.K. Burnham, J.M. Criado, L.A. Perez-Maqueda, C. Popescu, N. Sbirrazzuali, Thermochim. Acta 520 (2011) 1.
[53] W.A. Rosser, S.H. Inami, H. Wise, Combust. Flame 12 (1968) 427.
[54] N.E. Ermolin, O.P. Korobeinchev, A.G. Tereshenk, V.M. Foomin, Combust. Explos. Shock Waves 18 (1982) 180.
[55] G. Singh, I.P.S. Kapoor, D.K. Pandey, J. Energy Mater. 20 (2002) 223.